



Multi-analytical methodology to diagnose the environmental impact suffered by building materials in coastal areas

Olivia Gómez-Laserna¹ · Paola Cardiano² · Marta Diez-García¹ · Nagore Prieto-Taboada¹ · Leire Kortazar¹ · María Ángeles Olazabal¹ · Juan Manuel Madariaga¹

Received: 16 June 2017 / Accepted: 17 November 2017 / Published online: 27 November 2017
© Springer-Verlag GmbH Germany, part of Springer Nature 2017

Abstract

This work is focused on the development of an innovative multi-analytical methodology to estimate the impact suffered by building materials in coastal environments. With the aim of improving the in situ spectroscopic assessment, which is often based on XRF and Raman spectrometers, diffuse reflectance infrared Fourier transform (DRIFT) spectroscopy was implemented in the diagnosis study. In this way, the additional benefits from DRIFT were compared to the usual in situ analyses of building materials, which often have interferences from fluorescence and reststrahlen effects. The studies were extended to the laboratory scale by μ -X-ray fluorescence (μ -XRF) cross-section mapping and ion chromatography (IC), and the IC quantitative data were employed to develop thermodynamic models using the ECOS-RUNSALT program, with the aim of rationalizing the behavior of soluble salts with variations in the temperature and the relative humidity (RH). The multi-analytical methodology allowed identification of the most significant weathering agents and classification of the severity of degradation according to the salt content. The suitability of a DRIFT portable device to analyze these types of matrices was verified. Although the Kramers-Kronig algorithm correction proved to be inadequate to decrease the expected spectral distortions, the assignment was successfully performed based on the secondary bands and intensification of the overtones and decreased the time needed for in situ data collection. In addition, the pollutants' distribution in the samples and the possible presence of dangerous compounds, which were not detected during the in situ analysis campaigns, provided valuable information to clarify weathering phenomena.

Keywords In situ · Raman spectroscopy · DRIFT · μ -X-ray fluorescence mapping · Soluble salts · Thermodynamic model

Introduction

Currently, the economic potential of heritage buildings is widely recognized due to their status as an essential resource for cultural tourism and revalorization for educational

purposes (COM 2014). For sustainable preservation, the assessment of the conservation state must include a precise scientific diagnosis, and the characterization, interpretation, and classification of damage mechanisms suffered by building materials are crucial (Siegesmund and Sneath, 2011; Cardiano et al. 2008). To this end, the intrinsic and extrinsic factors influencing lithic materials' durability, such as petrographic characteristics, pollutants, and climatic conditions must also be considered (ASTM International 1998; Doehne and Price, 2010; Graue et al. 2013).

From an analytical point of view, this work is challenging, since sampling is sometimes restricted to preserve the integrity of the materials, and non-invasive studies that hinder correct data interpretation are required. Thus, non-destructive in situ techniques have been extensively tested in recent years (Pérez-Alonso et al. 2004; Giakoumaki et al. 2006; Hopkinson et al. 2015). In the field of spectroscopy, the combination of X-ray fluorescence (XRF) and Raman spectroscopy is one of the most employed due to its high chemical

Responsible editor: Santiago V. Luis

Electronic supplementary material The online version of this article (<https://doi.org/10.1007/s11356-017-0798-0>) contains supplementary material, which is available to authorized users.

✉ Olivia Gómez-Laserna
olivia.gomez@ehu.eus

¹ Department of Analytical Chemistry, University of the Basque Country (EHU/UPV), Barrio Sarriena s/n, E-48080, Leioa, Bilbao, Spain

² Department of Chemical, Biological, Pharmaceutical and Environmental Sciences, University of Messina, Viale F. Stagno d'Alcontres 31, I-98166 Messina, Italy

specificity, allowing in situ collection of a large amount of data in a relatively short time (Andrikopoulos et al. 2006; Gómez-Laserna et al. 2013). Although Raman spectroscopy is a suitable tool for the in situ analysis of a wide range of building materials (Hopkinson et al. 2015; Dariz and Schmid, 2017; Gázquez et al., 2017), the acquisition of clear spectral signals is mainly compromised by fluorescence effects, which are often caused by the presence of clay or organic matter and dust incorporated into the material due to external agents (Colomban, 2011; Tournié et al. 2011). In addition, specific weather conditions, such as temperatures, humidity, or strong sunlight, can complicate the analysis, increasing the number of required measurements and the time spent on data collection and processing (Aramendia et al. 2012). Although some radical methods, such as photobleaching, i.e., overexposure to a laser for a period of time to reduce the fluorescence intensity (Barman et al. 2011), can be exploited to gain more information, the use of other molecular techniques with new portable devices can improve the analytical methodology and reduce possible drawbacks. Accordingly, Fourier transform infrared spectroscopy (FTIR) is reported to be a suitable tool to investigate several materials, such as pigments (Fraquelo et al. 2009), binders (Sarmiento et al. 2011), documents (Bicchier et al. 2011), and marbles (Anselmi et al. 2011). Its use in diffuse reflectance mode (DRIFT) has been successfully applied in situ in this field (Arrizabalaga et al. 2014), leading to fewer spectral distortions arising from the optical impossibility of a portable device to separate the diffuse component from the specular one, known as the reststrahlen effect (Kortum 1969).

Furthermore, in situ spectroscopic methodologies are also often associated with laboratory analytical techniques, such as ion chromatography (IC), for the determination of soluble salts because they are known to be among the most significant causes of building deterioration (Flatt et al. 2014; Gomez-Laserna et al. 2015). Multivariate analysis and thermodynamic modeling of quantitative data can establish the chemical mechanism involved in degradation (Benavente et al. 2015; Prieto-Taboada et al. 2013; Veneranda et al. 2016).

In this work, an innovative multi-analytical methodology for the in situ characterization of lithic materials has been tested with the aim of minimizing the drawbacks of using Raman spectroscopy on this type of sample (Aramendia et al. 2012; Vítek et al. 2013; Medeghini et al. 2014) and increasing the amount and quality of the collected data. This approach provides adequate data for specialists making decisions about rehabilitation processes with a minimal impact on the heritage building.

For this purpose, the study consisted of different phases. First, the in situ analysis was based on a combination of X-ray fluorescence, Raman spectroscopy, and diffuse reflectance infrared Fourier transform (DRIFT). The advantages of DRIFT implementation to the in situ analyses to increase the

molecular information obtained in this type of matrix were evaluated, and the Kramers-Kronig algorithm was applied to correct the specular component contribution and minimize the expected spectral distortions due to the oxyanion content of the samples.

Then, to improve the methodology, an analysis was performed on the laboratory scale via implementation of μ -X-ray fluorescence (μ -XRF) as a micro-invasive mapping technique to obtain a large amount of information on the elemental distribution and penetration of deteriorating agents with a cross-section analysis (Jiménez Roca et al. 2005; Prieto-Taboada et al. 2013).

Once the “origin” of the damage was proposed on the basis of the spectroscopic data, the salt content was quantitatively determined by ion chromatography to ascertain the most important weathering agents involved in the degradation phenomena. In this way, the presence of chemical species dangerous to the long-term stability of stone materials but not detected by spectroscopic techniques was assessed (Gómez-Laserna et al. 2015); the severity of the damage was classified according to the guide issued by Fraunhofer-IRB (Auras 2011).

Finally, to provide a complete picture of the possible risks from the presence of soluble salts in the stone materials, their behavior was studied under various climatic conditions using the ECOS-RUNSALT program (Price 2000; Sawdy and Price, 2004; Sawdy and Price, 2005; Bionda 2005).

Materials and methods

Features of the case study

Building location and site climatic conditions

The Fishermen’s Association building is located in the center of the emblematic Donostia dock promenade (Gipuzkoa) (Fig. A1) approximately 5 m above sea level, and its back facade is directly attached to Urgull’s hill, which is a landscape area with great cultural value.

The climate in the city is classified as Atlantic (Cfb, Köppen-Geiger), and the average annual temperatures are 19 °C max/10 °C min with a rainfall of 1400 mm. Atmospheric humidity is high year-round with an average of 87% max/73% min. Moreover, due to the marine influence, days with fog and wind are very common (Kottek et al. 2006; www.euskalmet.euskadi.net).

According to the latest reports from the Basque Government, Donostia’s atmosphere shows medium pollution levels (annual average values of $PM_{10} = 23 \mu\text{g}/\text{m}^3$, $NO_2 = 30 \mu\text{g}/\text{m}^3$, $SO_2 = 35 \mu\text{g}/\text{m}^3$, and $O_3 = 54 \mu\text{g}/\text{m}^3$) and is classified as one of the least polluted cities in Spain (www.ingurumena.ejgv.euskadi.eus). However, port traffic may have increased the concentration of anthropogenic pollutants deposited on the building materials, which are mainly

coal, lead, and SO₂ from boat fuel and metals, such as iron and copper, due to the metallurgical commercial activities of the site.

Description of the building

The building was built in the twentieth century. Its structure remained unchanged until some detachment from Urgull’s hill occurred, and the building and surroundings suffered damage. In accordance with the Artistic Elements catalog of historical interest of the city (gipuzkoakultura.net/; www.donostia.eus/), the building was renovated under the secondary protection grade regulation; i.e., no esthetic changes were made in the facades and balconies, and maintenance was limited to consolidation or cleaning (BOPV 2002).

The back of the building is attached to the side of the Urgull hill. The front facade, which is oriented to the south-east, faces the dock promenade and the port. It has three levels above the ground plus the roof, which has a symmetrical composition altered with a transverse wink, and the main entrance is

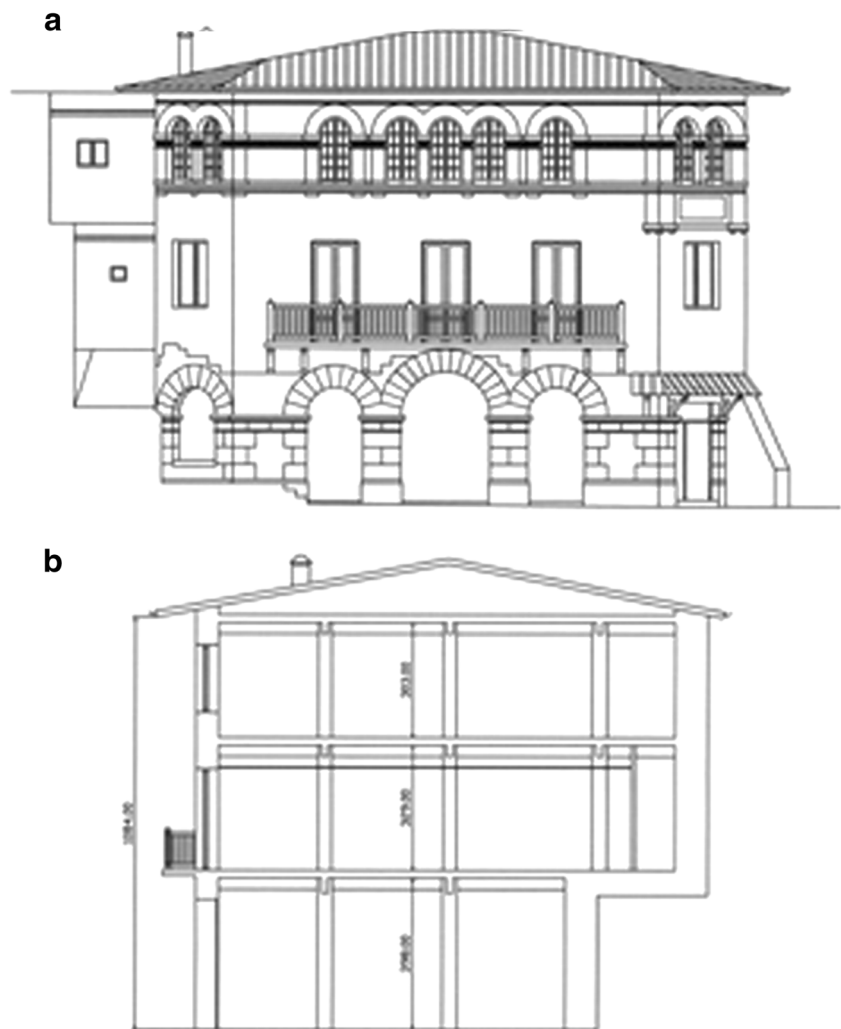
located on the ground floor (Fig. 1). The ground floor is used as a garage and is composed of masonry sandstone ashlars on a bed of limestone. The interior wall, which is adjacent to the hill, has a layer of lining mortar coated with white plaster. The facades of the first and second floor are also coated with white plaster. In the same way, the cover is composed of wood and carved concrete corbels, and the structure contains pillars and slabs of reinforced concrete, using the facade walls and gutters as support elements.

According to the last rehabilitation project, the original sandstone is from the Igueldo quarry (Gipuzkoa). Since various studies have been performed on these stones, their petrographic features and responses to different laboratory tests are well known (Rodríguez-Maribona et al. 1999; García-Garmilla et al. 2002).

Visual inspection

The building rehabilitation project was ongoing during the study; accordingly, the visual inspection focused on

Fig. 1 Elevation and cross-section planes of the Fishermen’s Association building. **a** Southeast from facade. **b** Cross section in which the different floor levels can be seen



identifying the main degradation phenomena and assessing their degree of severity. The areas available for the investigation were the facade, ground floor garage, and third floor. Due to the disrepair of the undercover supporting floor structure, access with portable equipment was not possible, and therefore, its study was performed by sampling. Accordingly, during visual inspection, various types of degradation were identified and classified as follows.

In the facade, the joint mortar was missing, and sandstone ashlars showed severe material loss, especially on the west and south sides, which are the most exposed to wind and rain. This material featured different degradation morphologies, such as flaking, disintegrations, and alveolizations. In addition, several salt efflorescences and subefflorescences were heterogeneously distributed and were more evident at the main entrance and on the southwest side (Fig. 2a–e).

In addition, on the balcony and areas exposed to water seepage from the roof, several detachments and cracks in the concrete structure were observed (Fig. 2g–h). The degradation was even more noticeable in the lower part of the balcony and the roof structure where the poor conservation state could cause the release of large shards. Several remediation attempts in the interior pillar were observed; nevertheless, the later reinforcement of the protective concrete layer appeared damaged, causing exposure of the structure to further deterioration. Thus, despite these conservation attempts, the corrosion of steel was still in progress.

In contrast, the masonry wall on the ground floor was wet and contained salt efflorescences. According to the last restoration project, the wall is 1.5 m thick and in direct contact with the Urgull hill. Therefore, it is the external building part and, in turn, the retaining wall on the hillside. However, several putlog holes for water drainage from the mountain exist (Fig. 2f).

In situ analysis campaign

Given this visual inspection, a first in situ analysis campaign was performed in October (2014). More than 100 measurements were collected by XRF, Raman, and DRIFT on non-damaged and damaged areas to confirm the composition of the original building materials and to identify the compounds due to degradation phenomena. During the study, measurements of the temperature and relative humidity were taken on site using a hygrometric (17–20 °C and 71–73%, respectively) as additional information to be considered for the thermodynamic modeling of the quantitative IC data.

In May, after several rainy days, a second analysis campaign was performed to detect possible variations caused by the change in the season. This time, more than 150 spectroscopic measurements were collected to study in detail the specific degradation phenomena. As mentioned before, temperature and relative humidity (22–25 °C and 72–80% RH) measurements were taken on site.

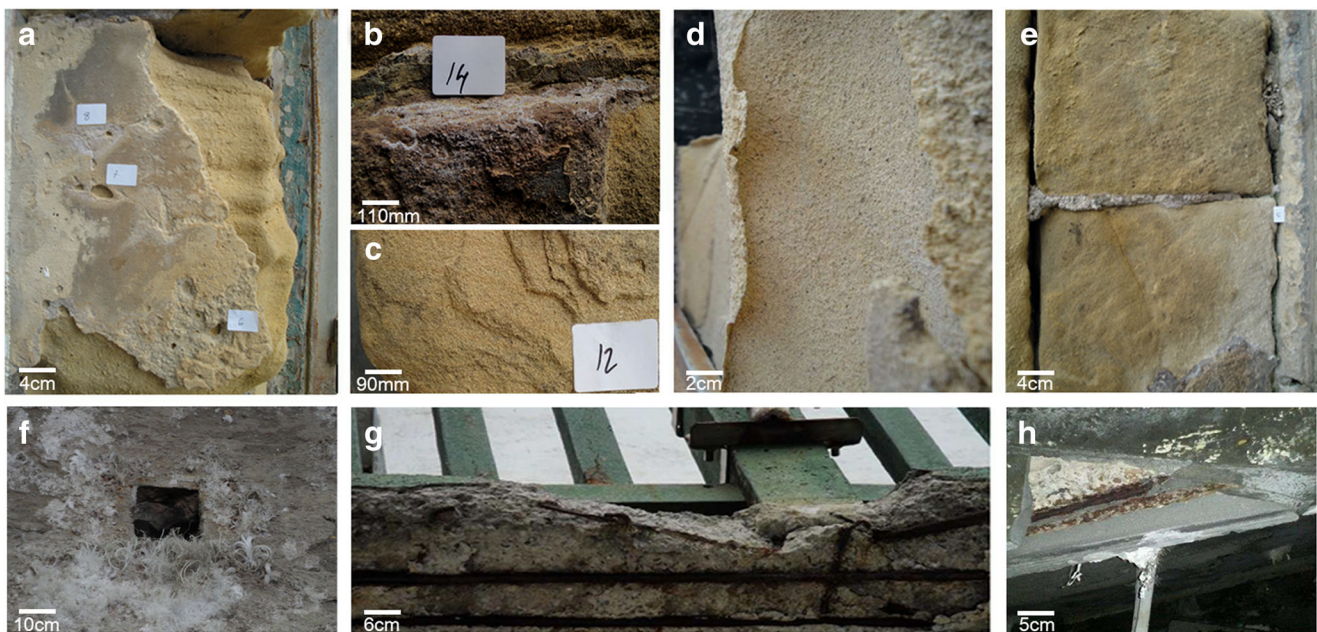


Fig. 2 Selected photographs of the degradation morphologies observed in the facade of the Fishermen's Association. **a, b, c, d,** and **e** Sanding, efflorescences, flaking, disintegration of ashlars, and lack of joint mortars detected on the facade. **f** Strong salt precipitation around putlog holes of

the masonry wall of the ground floor. **g** and **h** Balcony structure completely exposed to the atmosphere and detachment of the roof structure, where the pristine concrete and new concrete reinforcement can be observed

Sampling for the laboratory analysis

As a result of the first in situ study, during the second in situ campaign (May), very small amounts (approx. 0.13 g) of non-degraded sandstone were collected from a range of heights (Table A1) following the Italian guidelines (Normal 3/80) (C.N.R.-I.C.R. 1980) to confirm the composition of the original samples on the laboratory scale.

Moreover, selected degraded samples (efflorescences, sandstones, mortars, and detached layers of structural elements) from the facade, garage, and lower part of the balcony (Fig. 2g) were collected using a chisel (from 0.1 to 0.4 g of each one) to continue the diagnosis study in the laboratory (Table A1). All samples were registered and stored in zipped bags.

Due to differences observed in the results of the in situ spectroscopic analyses, eight additional sandstone samples were collected in July from the same points previously selected for analysis in the laboratory.

In addition, to determine the composition of the runoff coming from the mountain that could affect the conservation state of the building, soil, rain, and standing water samples were taken from the part adjacent to the hill to investigate their influence on the observed degradation. Approximately 250 mL of rain water and 50 mL of standing water were collected in a laboratory glass bottle, at 72 and 48 h, respectively. The samples were registered and stored at 4 °C.

Instruments and methods

In situ equipment

To determine the elemental composition, a semiquantitative in situ analysis was performed using a portable XRF spectrometer (X-MET5100 model, Oxford Instrument, UK). The calibration was performed using the method of fundamental parameters (FP) for different types of materials (non-standard calibration).

The molecular composition of the construction materials was investigated using a handheld Raman spectrometer (InnoRam, B&WTEK Inc., Newark, USA). The spectrometer uses a 785-nm laser of variable power to control thermal decomposition. The probe enables microscopic analysis using optical lenses ($\times 5$, $\times 20$, and $\times 50$), allowing the measurement of areas with diameters between 10 and 200 μm . A daily calibration was made employing a silicon chip. The spectra were collected in a fixed spectral range from 3000 to 175 cm^{-1} with a resolution of 3.5 cm^{-1} , using integration times from 1 to 8 s and 5 to 40 accumulations to improve the signal-to-noise ratio. Data acquisition was performed using the software B&WTEK Version 3.26 (Newark, USA).

In situ diffuse reflectance spectra were collected with a handheld FTIR spectrometer (4100 Exoscan, Agilent, Santa

Clara, USA) with a diffuse reflectance sampling interface recording short acquisition times and 32 accumulations. The Michelson interferometer features a maximum resolution of 4 cm^{-1} and a maximum spectral range of 4000–600 cm^{-1} . The background was acquired with a diffuse gold reference cap.

All in situ measurements were acquired with the portable instruments used directly on spots of the different materials; the spectra were processed with the Omnic version 7.2 software Thermo Nicolet (Madison, WI, USA), and their interpretation was achieved using the e-VISART, e-VISARCH, and e-VISNICH spectral databases (whose data were collected in our laboratory) as well as the RUFF (Castro et al. 2005; Pérez-Alonso et al. 2006; Downs 2006; Maguregui et al. 2010; Arrizabalaga et al. 2015).

Laboratory equipment

To gain more information from the cross-section analysis, the elemental mapping composition of the samples was analyzed in the laboratory using a μ -XRF spectrometer (ArtTax, Rontec, now Bruker AXS, Berlin, Germany). To obtain a focused spectroscopic image, polishing was achieved using a polisher (Forcipol@1, Metkon, Turkey). In addition, to avoid the dissolution of soluble salts, no water was employed in the process. A 50-kV voltage, 0.6-mA current, 1000 s, and a 0.65-mm tantalum collimator were used as the measurement conditions. The instrument is equipped with a molybdenum X-ray tube, a special Xflash detector (5 mm^2), and a measuring head implemented on a CCD camera that allows focusing on the sample using a motorized XYZ positioning unit controlled by the computer. Prior to the analysis, the equipment was calibrated with a bronze standard. Moreover, to identify the lightest elements, a helium flow was used.

All spectral processing and manipulations were performed using the ArtTAX software version 4.9.13.2 (Bruker AXS, Berlin, Germany). In addition, the program can perform automatic elemental maps because of the monitored movement of the axes. Color gradient graphs of the information were obtained using the Surfer software version 10.7.972 (Colorado, USA).

For the soluble salt determination, the selected samples were treated in triplicate following an ultrasound-assisted extraction method (Prieto-Taboada et al. 2012), which is an effective alternative to the standard EN 16455/2014 procedure. For each sample, 0.1 g was suspended in 100 mL of MilliQ water. The samples were introduced in an ultrasound bath for 2 h with a frequency of 40 kHz. For the extract filtration, Millipore 0.45- μm PTFE disc filters were used, and the solutions were stored at 4 °C, in polypropylene tubes until the analysis. To extract the soluble salts from the soil samples, the collected samples were lyophilized and sieved to a 500- μm mesh size to select the smallest particle fraction from the soil. The samples were treated in triplicate following a

reference method similar to EPA 300.0. (Schreiber et al. 2005). In this way, MilliQ water was added in a ratio of 1:10 (soil:water). The samples were sonicated in an ultrasound bath with a constant temperature of 20 °C for 10 min, and the extracts were filtered using Millipore 0.45- μm PTFE disc filters and stored in polypropylene tubes at 4 °C.

Quantitative determination of the soluble salts was achieved using a Dionex ICS 2500 suppressed ion chromatograph with an ED50 conductivity detector. For anions, an IonPac AS23 (4 \times 250 mm) column and an IonPac AG23 (4 \times 50 mm) precolumn were used, and, as the mobile phase, a solution of 4.5 mmol/L Na_2CO_3 /0.8 mmol/L NaHCO_3 was selected. The current and flow suppression conditions were 25 mA and 1 mL min^{-1} , respectively. The analysis of cations was conducted by an IonPac CS12A (4 \times 250 mm) column and IonPac CG-12A (4 \times 50 mm) precolumn from Vertex. As a mobile phase, a solution of 20 mmol/L CH_4SO_3 was used. The suppression current and flow were 50 mA and 1 mL min^{-1} , respectively. Data processing was performed by the Chromeleon version 6.60-SPIa software Dionex Corporation (Sunnyvale, CA, USA).

Results and discussion

In situ results

X-ray fluorescence

As expected, the elemental analysis of sandstone showed, Si as the main element, followed by Ca, Al, K, and Cl in lower proportions. Moreover, S, Fe, Ni, and Cu were identified as minor elements. The remaining part corresponded to light elements, mainly Na and O, since their signal was too low to be detected by the portable equipment employed.

According to the visual appearance of the samples and the elemental percentages detected, the results were in agreement with the data from the rehabilitation project, which indicated the use of glauconitic subarkose sandstone, which is very abundant in Donostia quarries and typical in historical buildings. It features a high percentage of fragmentary quartz as the main constituent of the cement (Fregenal et al. 2000). Calcium carbonate could be considered the minority cement as well as other chemically unstable compounds, such as feldspar, plagioclases, and glauconite grains, which are included in its composition to explain the presence of Al or Na (Rodríguez-Maribona et al. 1999; García-Garmilla et al. 2002).

Analysis of the joint mortars of the facade showed Si as the major element, Ca as the second element, and K, Al, S, and Cl in minor proportions. In addition, a small amount of Ni was detected. As already mentioned, the remaining part could correspond to other light elements, such as Na and O, whose assigned percentages were lower than 8%. The obtained

characterization matched the visual appearance of the cement mortars.

The lining mortar analyses from the masonry wall located in the garage could not provide an exhaustive characterization since the wall was completely covered by efflorescences, and therefore, the elemental analysis did not represent the composition of the original material. However, its visual appearance and the information detailed in the rehabilitation project indicated that the mortar used was based on Portland cement.

In addition, considering the location of the building and the detection of Ni and Cu, elemental mapping analyses were recommended to assess the penetration of toxic metals inside the building materials.

Finally, XRF analyses were performed on the same points selected for Raman and DRIFT in situ measurements to obtain additional information to facilitate the interpretation of the collected spectra.

DRIFT and Raman spectroscopy

According to the in situ Raman analysis on sandstones, α -quartz (α - SiO_2 , main peak at 465 cm^{-1} and secondary at 263 cm^{-1}), calcite (CaCO_3 , characteristic peak at 1085 cm^{-1}), and microcline (KAlSi_3O_8 , characteristics bands at 512, 475, 456, and 288 cm^{-1}) were identified as the original material components (Fig. 3).

The collected DRIFT spectra showed inverted bands (Fig. 4); the Kramers-Kronig algorithm was used to correct the reflectance measurement distortions (Kortum 1969). In this case, the roughness of the sample surface increased the

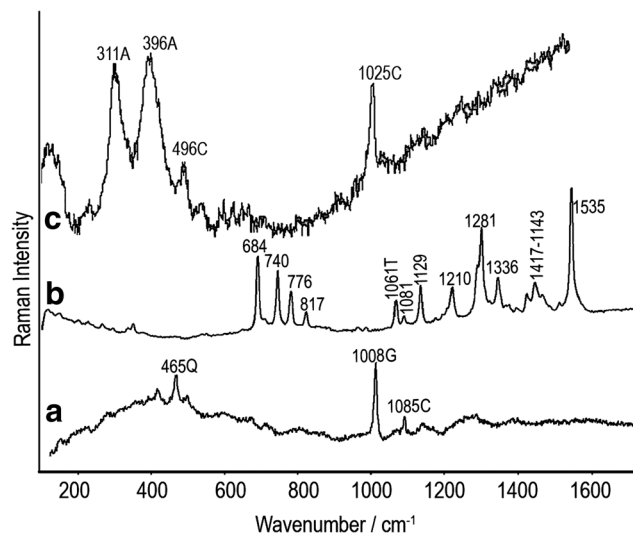


Fig. 3 (a) In situ spectrum showing the presence of calcite (C) and α -quartz (Q) as main original compounds of the sandstone; in addition, gypsum (G) could be observed as its direct degradation product. (b) Trona (T) and Winsor & Newton green pigment (G) could be observed as its direct degradation product. (c) Spectrum in situ collected over the interior structures; the signals of akaganeite (A) and coquimbite (C) can be observed

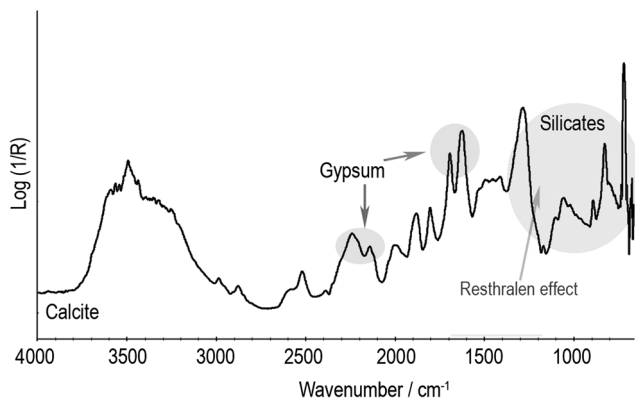


Fig. 4 DRIFT spectra of calcite and silicates in situ identified as original sandstone materials and secondary signal for gypsum

absorption index ($k \gg 1$). As a consequence, the intensity of the reststrahlen effect, which is related to the salt contents, such as carbonates, sulfates, and silicates, was too high to successfully remove the inverted bands, making the spectra interpretation difficult. Since more reflections in the reflectance measurements occur than in the transmittance mode, the overtones and combination band intensities increase, allowing the correct assignment of in situ collected spectra in most cases (C. Miliani et al. 2012). Accordingly, the data from the DRIFT analysis confirmed the composition of the original materials using secondary bands and overtones, and the reststrahlen effect distorted the spectra at approximately 1000 cm^{-1} (Si-O asymmetric stretching of silicates) and $1400\text{--}1500 \text{ cm}^{-1}$ (CO_3^{2-} asymmetric stretching). In this way, calcite (identified by its secondary bands at 2869 , 2513 , and 1795 cm^{-1}) and silicates (detected by their characteristic bands at approximately 1000 and $3500\text{--}3600 \text{ cm}^{-1}$) were found (Fig. 4). These results were in agreement with the subarkose sandstone composition; furthermore, as known from literature reports (Rodríguez-Maribona et al. 1999; García-Garmilla et al. 2002), the absorption and suction indexes according to RILEM are rather high at approximately 5.2% and $0.092 \text{ g cm}^{-2} \text{ min}^{-1}$, respectively, explaining the cement dissolution. The pore distribution system of this stone (porosity of 23.42% and pore diameter of $2 \times 10^4 \text{ nm}$) is thought to enhance water penetration through the material and facilitate the dissolution of the cement. The easy weatherability of this stone is also confirmed by its poor resistance against salt crystallization in the RILEM tests V.1 and V.2, (80.4% weight loss), which are closely related to water migration inside the lithic material (RILEM 1978; Rodríguez-Maribona et al. 1999).

However, spectroscopic analysis on the facade joint mortars revealed the presence of calcite (detected by its principal peak at 1085 cm^{-1} and secondary at 712 cm^{-1}), α -quartz (detected by its main peak at 464 cm^{-1}), and hematite (α - Fe_2O_3 , identified by its bands at 403 , and 289 cm^{-1}) as the main compounds in the original material. As in the case

already discussed, the DRIFT analysis corroborated the main composition, also detecting calcite and silicates. Although a great quantity of spectral information was collected, not all signals were accurately identified due to the lack of databases for these measurements and matrices.

Once the original compounds were identified, the degradation compounds were studied.

From the analysis of the facade samples, gypsum ($\text{CaSO}_4 \cdot 2\text{H}_2\text{O}$, detected by its main Raman signal at 1008 cm^{-1}) (Fig. 3) and mirabilite ($\text{Na}_2\text{SO}_4 \cdot 10\text{H}_2\text{O}$, detected by its main peak at 989 cm^{-1}), one of the most dangerous sulfates for building materials (Rodríguez-Navarro et al. 2000; Tsui et al. 2003; Steiger and Asmussen, 2008), were identified as the main degradation compounds in the efflorescences and subefflorescences of the detached and disintegrated ashlars. Moreover, calcite (detected by its main band at 1085 cm^{-1}) and trona ($\text{Na}_3(\text{HCO}_3)(\text{CO}_3) \cdot 2\text{H}_2\text{O}$, detected by its principal peak at 1061 cm^{-1}) were also found but in lower proportions and mainly detected in the joint mortars (Fig. 3). The DRIFT analysis on the same points confirmed the presence of calcite (by its bands at 2869 , 2514 , and 1795 cm^{-1}) and sulfate mixtures, and only gypsum (assigned to bands at 1682 and 1620 cm^{-1}) could be identified due to distortions induced by the reststrahlen effect. These compounds were classified as direct degradation products of the original calcite and silicates caused by atmospheric acid attack (Bai et al. 2003) as well as wet deposition of marine aerosols, which can enhance the transformation processes (Seo et al. 2007; Nikolaus et al. 2009). In addition to the loss of material by dissolution, this stone is known to be prone to salt crystallization decay (Rodríguez-Maribona et al. 1999), and the volume variations occurring during the dissolution-precipitation and hydration-dehydration processes could explain the visible deterioration and observed severe loss of material (Fig. 2a–e).

Furthermore, nitratine (NaNO_3 , detected by its characteristic Raman band at 1067 cm^{-1}) and probably niter (KNO_3), which were suggested by the K percentage observed in the XRF measurements (detected by its bands at 1050 cm^{-1}), were also found despite the fluorescence effect in the efflorescences and subefflorescences of the west side of the facade. The wet areas were also involved in the biodeterioration. The DRIFT analysis showed the presence of both degradation compounds by the identification of niter (DRIFT bands at 2735 , 2396 , 2066 , 1760 , 1491 , and 826 cm^{-1}) and nitratine (determined by its bands at 2757 , 2435 , 2096 , 1786 , 1535 , and 836 cm^{-1}). However, nitrates were only found during the first in situ campaign. Considering that this side of the facade is completely exposed to the rain, wet to the touch, and growth of vegetation is only observed in this area, the nitrates' presence could be explained as a consequence of the attack of atmospheric gases on the silicate compounds and worsened by root action, which can promote the infiltration of water and contribute to the dissolution.

Finally, it is worth mentioning that some green particles are heterogeneously distributed on the lower ashlar. Although, in the past, this part was painted, the color was removed to leave the stone exposed and to preserve the architectural ensemble of the houses surrounding the building. The traces of this coloration were identified as Winsor & Newton green pigment (by its Raman bands at 1535, 1143, 1417, 1336, 1281, 1210, 1129, 1081, 817, 776, 740, 684 cm^{-1}) (Fig. 3).

In the interior wall of the ground floor, directly attached to the mountain, gypsum (identified by its main Raman band at 1008 cm^{-1}), mirabilite (main Raman band at 989 cm^{-1} and the weakest bands at 458 and 446 cm^{-1} aside from 1130, 1120, 1108, 628, and 616 cm^{-1}), thenardite (Na_2SO_4 , identified by the strongest peak at 993 cm^{-1} and the weakest pair of peaks at 466 and 451 cm^{-1} aside from signals at 1149, 1128, 644, 632, and 621 cm^{-1}), nitrocalcite ($\text{Ca}(\text{NO}_3)_2 \cdot 4\text{H}_2\text{O}$) (identified by its Raman at 1050 and 719 cm^{-1}), niter (detected by its main peak at 1050 and its secondary bands at 1359, 1344, and 715 cm^{-1}), and nitratine (identified by its Raman bands at 1067 and 724 cm^{-1}) were detected as the main components of the efflorescences. These results were confirmed in situ by the DRIFT identification of several mixtures of sulfates and nitrates. However, the wet surface of some areas of the wall together with the surface characteristics showed a negative influence on the collected DRIFT spectra. Some drawbacks related to the saturated measurements also occurred, making the data collection difficult.

The origin of the high amount of salt is strictly related to the water infiltration from the hill, which is in direct contact with this wall (1.5 m thick). The water was a charged leachate and passed through the wall due to the porous network, causing dissolution of the original materials on the surface. In addition, this weathering phenomenon could even be enhanced by the plaster layer covering the entire wall. This layer is dissolved by the action of the infiltrated water, increasing the amount of sulfates in solution and the amount of sulfated efflorescences. Furthermore, the pressure exerted by the different crystallization processes results in a detachment of the layer, revealing the presence of subefflorescences.

Due to the interior location of the wall, the abundance of nitrates may be explained in terms of two possible sources, i.e., water infiltration from the mountain and water from the ground by capillary action, and organic matter decomposition can occur (Matović et al. 2012; Gázquez et al. 2015). However, the contribution of the second option should be minor due to the bed of limestone and the concrete layer on which the building was built; these materials are often used as a barrier to avoid this type of damage.

The last area of interest was the internal structures which, due to the decay processes, were totally exposed to the open air (Fig. 2g–h). Raman analysis revealed the severity of degradation in this part of the building, and several iron oxides, such as hematite (assigned by its bands at 404, 289, and

223 cm^{-1}), akaganeite ($\beta\text{-FeO}(\text{OH})$, assigned by its Raman bands at 311 and 393 cm^{-1}) (Fig. 3), and lepidocrocite ($\gamma\text{-FeOOH}$, detected by its main Raman band at 250 cm^{-1}), were identified.

Moreover, coquimbite ($\text{Fe}_2(\text{SO}_4)_3 \cdot 9\text{H}_2\text{O}$, identified by its Raman peaks at 1025 and 496 cm^{-1}) (Fig. 3), gypsum (identified by its bands at 1008, 670, 493, and 414 cm^{-1}), and calcite (assigned by its main band at 1085 cm^{-1}) were also found as degradation compounds in the efflorescences located on the structures.

The layer of concrete that covers the internal structures features a certain durability, which is strongly influenced by environmental factors. Accordingly, in coastal atmospheres, it can be severely degraded by chlorides that can accelerate the corrosion process (Johansson et al. 1988). According to the Structural Concrete Instruction (EHE-08 1247/2008), some requisites should be fulfilled in buildings located near the sea. However, at the time of construction, these requirements were not taken into account, and the work performed during the rehabilitation project was meant to cover the damage with new layers of concrete rather than find a long-term solution for the degradation, regardless of the carbonation process. This chemical process is caused by a decrease in the pH inside the material due to the penetration of water and atmospheric CO_2 . The dissolved gas attacks the porous matrix, transforming the original calcium hydroxide, $\text{Ca}(\text{OH})_2$ into calcium carbonate, CaCO_3 . This causes vulnerability in the reinforced concrete. The protective oxide layer of reinforcement steel is achieved by passivation of its surface and is stable only in highly alkaline environments. If the carbonation process progresses and reaches the steel, the protective layer loses stability. In this way, at pH values below 11, corrosion begins and may induce cracking and spalling of the material (Saetta and Vitaliani, 2004; Chávez-Uloa et al. 2013). Consequently, the penetration of water and atmospheric pollutants into the lithic matrix is facilitated, and deterioration increases until the concrete layer bursts, leaving the internal structures completely exposed to the aggressive atmosphere.

The presence of calcite efflorescences confirms the severe degree of carbonation suffered by the structures. In addition, the identification of akaganeite is worth mentioning since a high concentration of chlorides in the surroundings of the iron piece is required for its formation, evidencing the loss of the passivation layer in the internal structures (Selwyn, 2004). According to the in situ study, this degradation phenomenon is one of the most dangerous, as it can affect the overall stability of the building. Furthermore, the detachment of the roof structure could cause worker injury due to falling debris in the office area. Moreover, the lower parts of the balconies also feature severe carbonation and are in danger of collapse. Since these elements were declared to be historical heritage, they require an urgent intervention.

Laboratory results

Mapping analysis by μ -XRF

According to the in situ results, the sandstone sample selected from the facade was prepared for cross-section analysis to avoid the loss of soluble and weakly anchored compounds. The elemental distribution was investigated to evaluate the pollutants' penetration depth and to define the restoration requirements, such as the cleaning procedures or the penetration capability of the consolidants.

Elemental mapping of the sample (Fig. 5) shows silicon as the main component of the cementitious matrix, which was homogeneously distributed. The areas with the lowest concentration of this element correspond to the highest levels of potassium and calcium. This evidence is attributed to the natural percentage of calcium carbonate and feldspars inherent in

the material. However, in the deepest areas, which correspond to a natural fracture, no element related to the cementer is observed, explaining the release of the sandstone piece. In the same way, the iron distribution is homogenous, as expected from the natural composition of the glauconitic grains. Lead is more concentrated in areas close to the surface, suggesting that its presence is due to anthropogenic sources, although the external areas can be washed by rain. The observed distribution of zinc was surprising since no compound of this type was expected. Although the fluorescence effect in the Raman measurements and the lack of standards in the DRIFT database can make identification difficult, the feldspar content of the subarkose sandstone is mainly related to potassium (Rodríguez-Maribona et al. 1999; García-Garmilla et al. 2002). Considering the strip was observed from 1.2 cm (Fig. 5), metallurgical activities are typical in the area and zinc is often used in galvanic and melting processes, the presence of

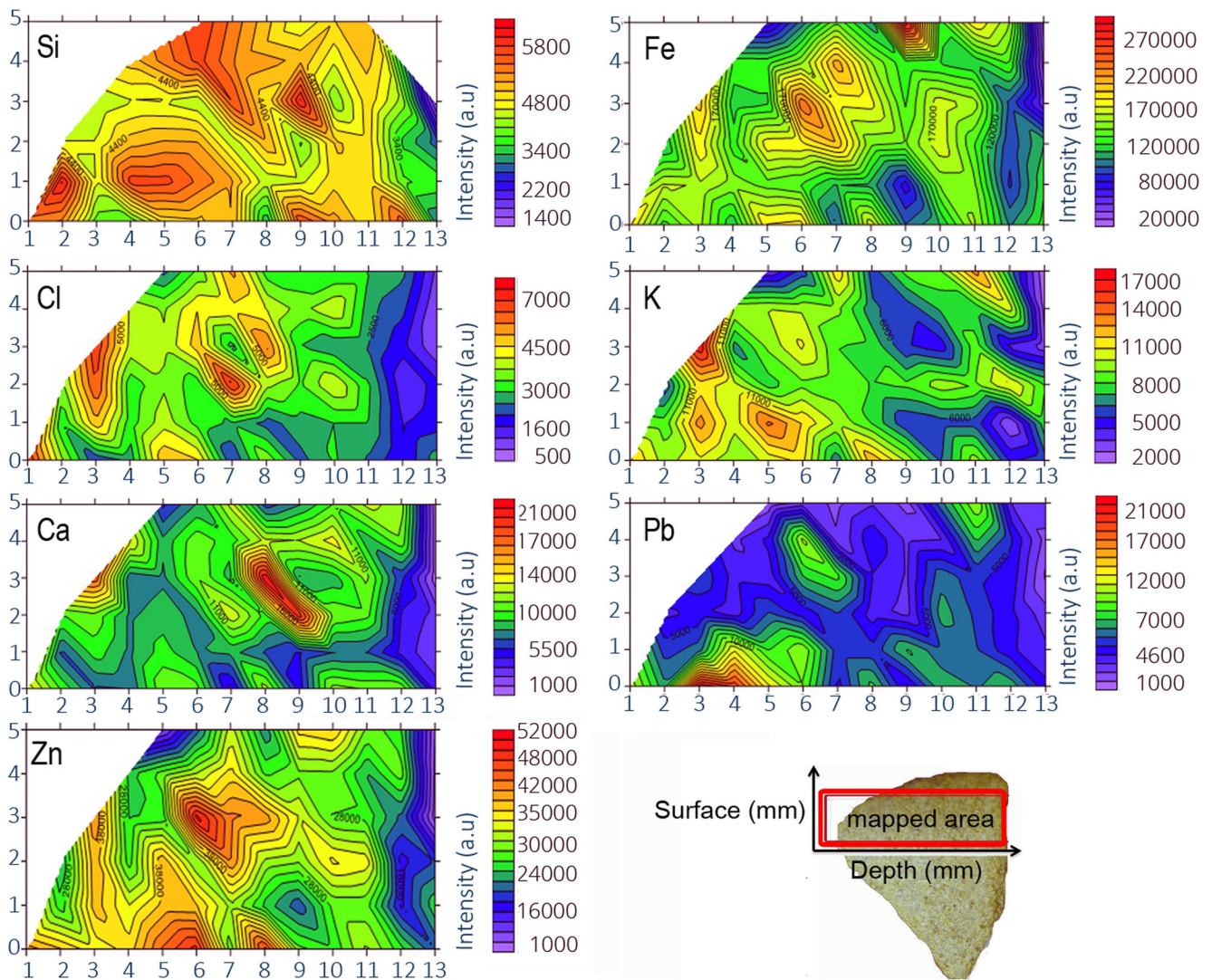


Fig. 5 Cross-section mapping analysis by μ -XRF of the sandstone sample using Surfer 10 software. The elemental distribution and abundance are shown

this element could be attributed to the deposition of particulate matter, which can be transported inside the outer strata of the lithic material by the action of water. In addition, the chloride levels clearly demonstrate marine aerosol deposition, evidencing its ability to penetrate the material.

This analysis showed the elemental distribution inside the material, and the relevant impact of external sources of deterioration, such as marine aerosols and metallurgical industry, were assessed.

Raman spectroscopy

Using the laboratory Raman analysis of the sandstone samples, the full spectra of α -quartz, calcite, and microcline were obtained, confirming the composition of the original materials (Fig. 6). In addition, glauconite ((K, Na) $(\text{Fe}^{3+}, \text{Al}, \text{Mg})_2(\text{Si}, \text{Al})_4\text{O}_{10}(\text{OH})_2$, assigned by the Raman bands at 1121, 1064, 680, 550, 463, 378, 350, 255, and 201 cm^{-1}) was also found as an original compound, corroborating the stone type. In the same way, calcite, gypsum, and mirabilite were identified as the main degradation compounds of the efflorescences and subefflorescences, evidencing atmospheric acid attack and the deposition of marine aerosols.

Moreover, in samples taken from the west side of the facade, which was mainly affected by biodeterioration, no nitrates were identified, which is likely due to sampling during the rainy season. However, in this area, glauconite ($\text{Na}_2\text{Ca}(\text{SO}_4)_2$ assigned by its Raman band at 1002 cm^{-1}) was found, complementing the spectroscopic analysis, even if only its main signal was detected due to the fluorescence effect. Again, calcite, gypsum, and mirabilite were identified as the main degradation compounds of the efflorescences and subefflorescences, confirming atmospheric acid attack and the deposition of marine aerosols.

The formation of this mixed sulfate is very common in medium rich in sulfate and chlorides. Accordingly, glauconite usually crystallizes together with mirabilite and halite. Due to

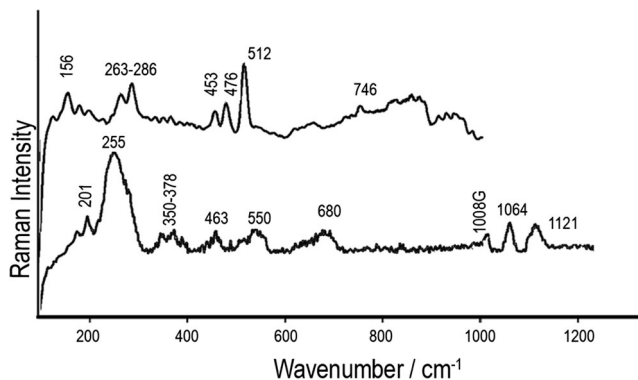


Fig. 6 In situ spectrum showing the presence of glauconite and gypsum (G) in the sandstone samples (lower part). In the upper spectrum, microcline signals can be observed

the noticeable amount of sulfates detected and the coastal environment, its presence was not surprising.

According to analysis of the samples collected from the interior wall of the ground floor, gypsum, mirabilite, nitrocalcite, and nitratine were identified as the main compounds of the salt crust layer. Furthermore, this time, the full set of signals of glauconite (Raman bands at 1140, 1106, 1002, 644, and 471 cm^{-1}) were found.

However, analysis of the samples collected in the internal structures confirmed the in situ results and identified hematite, akaganeite, lepidocrocite, and goethite (α - FeOOH , assigned by its Raman bands at 529, 475, 384, 300, and 248 cm^{-1}), which suggested the loss of the passivation layer due to the attack of marine aerosols.

Finally, the data collected on the efflorescence samples found on the structures showed that carbonation occurred, and calcite and kalicinite were identified (KHCO_3 , detected by its Raman bands at 1027, 637, and 188 cm^{-1}). Moreover, coquimbite, basanite ($\text{CaSO}_4 \cdot 0.5 \text{H}_2\text{O}$, Raman bands at 1015, 668, 627, 487, and 429 cm^{-1}), and bianchite ($\text{ZnSO}_4 \cdot 6\text{H}_2\text{O}$, Raman bands at 1025, 624, 423, and 284 cm^{-1}) were also found as minor compounds, which demonstrated the severity of this degradation phenomenon.

Quantification of the soluble salts by ion chromatography

Using ion chromatography, the ionic soluble components of the soil, rain, and standing water samples from the part adjacent to the hill were analyzed. According to the results for the rain water samples (Table 1), sulfates and sodium were the most abundant ions that penetrated the sandstone materials and the internal structures via the action of rain. The unbalanced ionic content detected likely indicates the presence of carbonates and bicarbonates, which cannot be quantified due to the mobile phase used in the analysis. Once again, these data show that the acid attack from atmospheric gases (by wet or dry deposition) can be envisaged as the main cause of degradation involving the original materials and explains their transformations into gypsum, mirabilite, coquimbite, and even trona.

Moreover, common fogs and marine aerosols can increase the concentration of ions, such as chlorides, in the atmosphere, promoting further corrosion, dissolution, and salt damage (Seo et al. 2007; Nikolaus et al. 2009).

The soil and standing water ionic soluble content support the hypothesis of runoff water infiltration as the main cause of degradation of the inner wall. As shown by the quantitative data, the rainwater can leach large amounts of nitrates, chlorides, and sulfates from the soil and drag them through the wall, inducing the severe saline degradation phenomenon observed.

To determine the salt content, the efflorescences, sandstones, and mortar samples taken during the second campaign

Table 1 Cation and anion concentration values in mg·kg⁻¹ and method repeatabilities, in RSD %, obtained by ion chromatography

Sample	Na ⁺	K ⁺	NH ₄ ⁺	Ca ²⁺	Cl ⁻	NO ₃ ⁻	SO ₄ ²⁻
Rain water	2.8 × 10 ³	<QL	<QL	<QL	<QL	<QL	1.44 × 10 ³
Standing water	3.1 × 10 ⁴	1.1 × 10 ⁴	1.2 × 10 ⁴	5.4 × 10 ⁴	5.6 × 10 ⁴	7.6 × 10 ³	2.1 × 10 ⁴
Soil	1.61 × 10 ³	3.1 × 10 ³	1.0 × 10 ³	4.4 × 10 ³	1.8 × 10 ³	2.5 × 10 ³	1.4 × 10 ³
RSD (%)	3	4	2	5	3	4	2

were analyzed by ion chromatography. In this way, soluble sulfate, nitrate, chloride, sodium, potassium, calcium, and magnesium concentrations were quantified (Tables 2 and 3). Moreover, the percentage of each anion was also calculated separately (Tables 2 and 3) to compare the salt levels considered potentially hazardous for porous materials according to the guide issued by Fraunhofer-IRB (Auras 2011). The guide classifies the damage severity in five grades (G0-Non-load, GI-Low load, GII-Medium load, GIII-Highly loaded, and GIV-Extremely loaded) using the chloride, nitrate, and sulfate contents. From the results, the sandstone samples collected on the facade displayed sulfates as the major compounds, but important amounts of nitrates were also found. According to the Fraunhofer-IRB classification, only samples 3S and 4S showed medium load levels. The remaining samples featured severe salts levels, reaching in most cases the highest grade of load (G-IV) (> 0.6 NO₃⁻ %, > 0.77 SO₄²⁻ %, and > 0.28 Cl⁻ %), which confirmed the high damage found in the sandstone ashlar.

However, the data from the mortar and efflorescence samples (Table 3) showed high amounts of chlorides and sulfates. Some chlorides are expected in sand mortars, and the high values observed could be only explained by sea spray deposition, which can easily penetrate the holes of the joint mortars and the cracks in the linings of the structures. In addition, the concentration was classified as “extreme grade” (G-IV) for all the samples, explaining the observed salt damage and the poor conservation state of the joint mortars.

Finally, the ion content of the efflorescences collected on the surrounding internal structures showed massive attack by

the sulfates and chlorides to which the structures are exposed and the consequent danger of this type of degradation.

Thermodynamic modeling: RUNSALT

Due to the variability in the salt formations observed during both the in situ spectroscopic investigations, the sandstone from the second sampling was analyzed by ion chromatography to study the behavior of the ionic soluble content.

For that purpose, soluble sulfates, nitrates, chlorides, sodium, potassium, calcium, and magnesium concentrations were quantified (Table 4).

In agreement with the previous results, the soluble salt contents of the sandstone ashlar were strongly influenced by the season, i.e., rainy or not. From the data comparison of both samplings (Fig. A2), a high increase in the chlorides and nitrates was observed, and the sulfates showed the opposite behavior.

As the spectroscopic techniques indicated, nitrates and chlorides mainly correlate with potassium and sodium, and the corresponding salts were highly soluble. Therefore, their dissolution by rain is more likely. In contrast, sulfates are mostly correlated with calcium, which creates less soluble salts, and thus, its concentration is more stable over the year. Furthermore, the concentration changes in the salt mixtures affect the balance of their formation, promoting sulfate formation during the rainy season.

In addition, to determine the influence of the relative humidity and temperature changes (www.euskalmet.euskadi.net) in the activation of the salt

Table 2 Cation and anion concentration values for sandstone samples in mg·kg⁻¹ and method repeatabilities, in RSD %, obtained by ion chromatography. Percentages of sulfate and nitrate can be seen

Sample	Na ⁺	K ⁺	Ca ²⁺	Cl ⁻	NO ₃ ⁻	SO ₄ ²⁻	Wt% (SO ₄ ²⁻)	Wt% (NO ₃ ⁻)
1S	–	–	1.7 × 10 ⁴	<QL	<QL	3.7 × 10 ⁴	3.7	–
2S	6.7 × 10 ³	<QL	2.2 × 10 ³	<QL	<QL	8.6 × 10 ³	0.8	–
3S	4.1 × 10 ³	<QL	1.1 × 10 ³	<QL	<QL	<QL	–	–
4S	2.7 × 10 ³	<QL	5.1 × 10 ³	<QL	5.6 × 10 ³	<QL	–	0.6
5S	5.3 × 10 ³	<QL	1.6 × 10 ⁴	<QL	9.3 × 10 ³	1.2 × 10 ⁴	1.2	0.9
6S	5.0 × 10 ³	<QL	7.6 × 10 ³	<QL	8.1 × 10 ²	1.0 × 10 ⁴	1	8.1 × 10 ⁻²
7S	2.7 × 10 ³	<QL	<QL	<QL	6.2 × 10 ³	8.2 × 10 ³	0.8	1.0 × 10 ⁻²
8S	<QL	<QL	7.8 × 10 ³	<QL	<QL	2.3 × 10 ⁴	2.3	–
RSD (%)	4	–	3	–	3	5	–	–

Table 3 Cation and anion concentration values for mortar and efflorescence samples in $\text{mg}\cdot\text{kg}^{-1}$ and method repeatabilities, in RSD %, obtained by ion chromatography. Percentages of sulfate and chloride can be seen

Sample	Na^+	K^+	Ca^{2+}	Cl^-	NO_3^-	SO_4^{2-}	Wt% (SO_4^{2-})	Wt% (Cl^-)
1J	5.7×10^4	2.4×10^3	1.6×10^4	8.8×10^4	–	1.0×10^4	1	8.8
2J	1.0×10^4	–	9.4×10^3	9.5×10^3	–	6.2×10^3	0.6	0.9
3J	2.3×10^4	–	1.8×10^4	4.2×10^4	–	7.3×10^3	0.7	4.2
1L	8.5×10^3	2.5×10^3	2.2×10^4	1.9×10^4	–	2.4×10^4	2.4	1.9
2L	1.5×10^4	2.2×10^3	3.0×10^4	2.2×10^4	–	5.6×10^4	5.6	2.2
1E*	3.3×10^5	–	1.2×10^4	5.2×10^5	–	–	–	51.9
2E*	4.1×10^5	1.9×10^3	3.2×10^3	7.1×10^5	–	–	–	70.7
1ES**	1.6×10^5	–	1.0×10^4	2.5×10^5	<QL	–	–	24.7
2ES**	1.2×10^5	–	2.6×10^4	–	<QL	4.0×10^5	40.3	–
3E**	6.6×10^3	–	1.8×10^4	2.0×10^4	–	7.0×10^3	0.7	2
4E**	5.3×10^3	–	1.6×10^4	–	–	1.9×10^4	1.9	–
5E**	1.8×10^5	–	3.8×10^4	1.8×10^4	–	5.8×10^5	58.6	1.8
*RSD (%)	5	3	4	6	–	5	–	–

* Efflorescence sample of mortars

** Efflorescence sample of internal structures

damage, the IC quantitative results of the samples collected during the driest months were studied using a thermodynamic predictive ECOS model (Price 2000; Sawdy and Price, 2004; Sawdy and Price, 2005; Bionda 2005). Considering the ionic balance of the samples was close to unity, the amount of calcium was adjusted according to the estimated equivalents of carbonate and introduced into the calculation. In this way, in cold months, the formation of gypsum and halite are expected at an average temperature of 10 °C. However, if the temperature increases up to 15 °C, the amount of gypsum and halite decreases, allowing the formation of new sulfate compounds, such as mirabilite, glauberite, and gormeyite ($\text{K}_2\text{SO}_4 \cdot 5\text{CaSO}_4 \cdot \text{H}_2\text{O}$). Finally, during the summer, nitrates are expected in the form of nitratine (Fig. 7). Accordingly, the 9S, 10S, 11S, and 12S samples showed similar behaviors. However, from the soluble salt content of sample 16S, other degradation compounds,

such as niter, sylvite (KCl), apthitalite ($\text{Na}_2\text{SO}_4 \cdot 3\text{K}_2\text{SO}_4$), hexahydrate ($\text{MgSO}_4 \cdot 6\text{H}_2\text{O}$), and picromerite ($\text{K}_2\text{SO}_4 \cdot \text{MgSO}_4 \cdot 6\text{H}_2\text{O}$), should be expected. Some expected compounds were also detected by spectroscopic techniques in the annual study, corroborating the suitability of this software as a complementary tool to correlate phenomenological, analytical, and environment information and to predict the presence of dangerous compounds that cannot be spectroscopically detected. The application of this study enabled the determination of building material damage associated with the crystallization and deliquescence of soluble salts, demonstrating that small temperature and RH changes are sufficient to activate salt damage cycles. Nevertheless, the thermodynamic model used cannot consider variations in concentrations caused by external factors, such as surface washing, industrial activity, fog, etc. Therefore, the collection of representative samples, considering

Table 4 Cation and anion concentration values for sandstone samples in $\text{mg}\cdot\text{kg}^{-1}$ and method repeatabilities, in RSD %, obtained by ion chromatography

Sample	Na^+	K^+	Ca^{2+}	Cl^-	NO_3^-	SO_4^{2-}	Mg^{2+}
9S	2.2×10^4	8.2×10^3	1.6×10^4	3.7×10^4	1.8×10^4	2.7×10^4	–
10S	4.3×10^3	6.5×10^2	4.9×10^3	6.2×10^3	3.2×10^3	2.2×10^4	–
11S	1.9×10^3	4.6×10^2	1.1×10^4	4.6×10^3	1.2×10^3	5.5×10^3	<QL
12S	1.7×10^3	3.9×10^2	5.7×10^3	3.7×10^3	1.1×10^3	8.0×10^3	–
13S	1.6×10^3	5.1×10^2	3.8×10^3	3.2×10^3	1.8×10^3	6.2×10^3	<QL
14S	1.2×10^3	3.8×10^2	1.9×10^3	2.8×10^3	8.4×10^2	2.7×10^3	–
15S	1.2×10^3	1.2×10^3	1.7×10^3	1.9×10^3	2.2×10^3	<QL	–
16S	1.0×10^3	2.6×10^3	2.8×10^3	1.8×10^3	1.9×10^3	7.0×10^3	4.2×10^2
RSD (%)	4	4	3	5	3	5	2

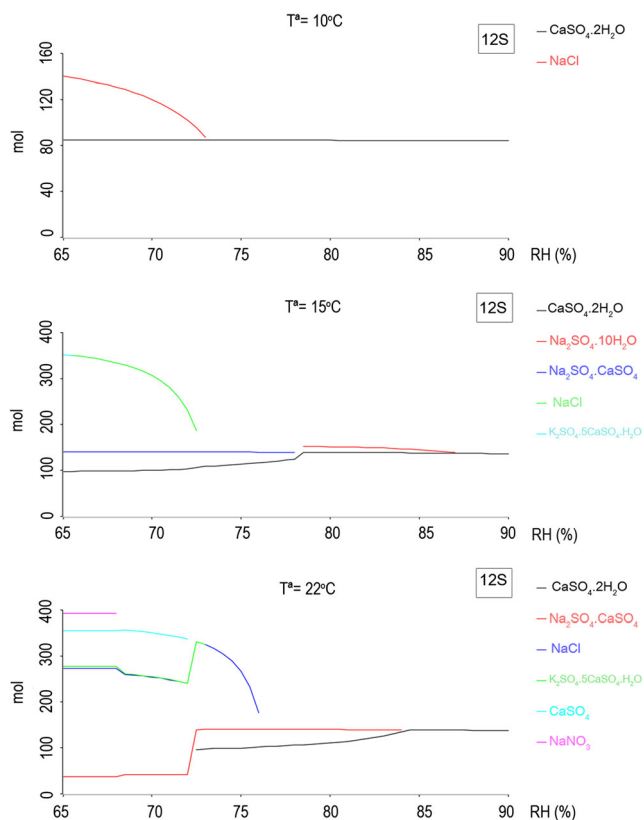


Fig. 7 Thermodynamic analysis using RUNSALT. Crystallization sequence of soluble salts extracted from sample 12S at **a** 10 °C, **b** 15 °C, and **c** 22 °C according to variable values of relative humidity

seasonal conditions, is crucial to improve the predictions. In addition, this tool could provide valuable information to indicate the best time of year to perform the in situ analysis, sampling campaigns, and conservation actions.

Conclusions

The work performed on the Fishermen’s Association shows how useful Raman spectroscopy can be as a main technique for the diagnosis of the state of conservation of historic buildings. In contrast, the effectiveness of DRIFT mainly depends on the morphological properties of the samples. The volume of reflections is influenced by the roughness of the surface and the increasing absorption index, and severe spectral distortions are observed. Thus, the inverted bands induced by the reststrahlen effect could not be corrected by post-processing with the Kramers-Kronig algorithm. Nevertheless, because the secondary bands and the intensification of the overtones have a smaller absorption index, the distortion is minor, allowing reliable spectral assignments. Samples with functional groups such as CO_3^{2-} , SO_4^{2-} , and NO_3^- showed combinations and overtone bands from 2600 to 1900 cm^{-1} , which

are suitable for molecular characterization and identifying the cation and hydration state. Unfortunately, it should be noted that the DRIFT database is not very extensive. Thus, although a considerable amount of salts were identified in the study, several signals of silicates were only assigned using the functional group and were not specifically identified due to the lack of standards. These compounds are usually related to the clay content, and therefore, the fluorescence effect in the Raman signal is stronger. The advantages addressed by the Raman and DRIFT combination may notably increase with the elaboration of more complete databases, decreasing the time spent on in situ data collection and further processing. The spectroscopic data actually established the causes of degradation based only on the in situ campaign results; the information obtained by the in situ Raman investigations was further validated by DRIFT. In addition, micro-invasive laboratory techniques are proposed to complete the multi-analytical methodology, allowing the assessment of the pollutant distribution inside the porous matrix, even for compounds undetectable by spectroscopy, such as chlorides, and enabling recognition of the role played by rain in building degradation and the thickness of the strata involved.

Moreover, the combination of spectroscopic techniques with quantitative analytical methodologies proved to be a good strategy to consider the presence of harmful compounds, which are otherwise not detectable, for preservation and to quantify the severity of the degradation they cause in accordance with existing regulations.

The spectroscopic results of the different campaigns were supported and completed using thermodynamic modeling. These data treatment can allow for faster diagnosis in future work, providing valuable information to indicate the best time of year to perform in situ campaigns without losing precious time to avoid further degradation. Moreover, it could help to select the best restoration materials, inhibitors, and consolidation products, and to avoid the ignorance of harmful compounds. This thermodynamic model could be very useful in the preservation of other types of buildings with cultural and historical value involved in soluble salt degradation, while increasing knowledge of the environmental factors influencing the decay.

Finally, the work performed shows the essential utility of scientific studies to rehabilitate heritage buildings, promoting interdisciplinarity. The information provided by this methodology could avoid the selection of improper conservation actions and, therefore higher costs. In fact, the minimal economic impact that the application of this methodology requires for a real restoration project is noteworthy. Unfortunately, these work protocols are not often requested, since among the architects’ community, a correct perception of their utility is still lacking. Because of the development of awareness promoted by ICOMOS, the current vision and standard methods in this field are changing.

Acknowledgements O. Gómez-Laserna and L. Kortazar, gratefully acknowledge their post-doctoral contract from the University of the Basque Country (UPV-EHU) and predoctoral fellowship from the Basque Government (GV/EJ), respectively.

Funding information This work has been financially supported by the project MADYLIN from the Spanish Ministry of Economy and Competitiveness (MINECO) (ref: BIA2017-87063-P) and by the European Regional Development Fund (FEDER)

References

- American Society for Testing and Materials (1998) Annual book of ASTM standards. ASTM International, West Conshohocken
- Andrikopoulos KS, Sister D, Roussel B, Janssens K (2006) In vitro validation of a mobile Raman-XRF micro-analytical instrument's capabilities on the diagnosis of Byzantine icons. *J Raman Spectrosc* 37(10):1026–1034. <https://doi.org/10.1002/jrs.1612>
- Anselmi A, Presciutti F, Doherty B, Brunetti BG, Sgammelli A, Miliani C (2011) The study of cyclododecane as a temporary coating for marble by NMR profilometry and FTIR reflectance spectroscopies. *Appl Phys* 104(1):401–406. <https://doi.org/10.1007/s00339-010-6170-6>
- Aramendia J, Gomez-Nubla L, Castro K, Martinez-Arkarazo I, Vega D, Sanz López de Heredia A, García Ibáñez de Opakua A, Madariaga JM (2012) Portable Raman study on the conservation state of four CorTen steel-based sculptures by Eduardo Chillida impacted by urban atmospheres. *J Raman Spectrosc* 43(8):1111–1117. <https://doi.org/10.1002/jrs.3158>
- Arrizabalaga I, Gómez-Laserna O, Aramendia J, Arana G, Madariaga JM (2014) Applicability of a diffuse reflectance infrared Fourier transform handheld spectrometer to perform in-situ analyses on Cultural Heritage materials. *Spectrochim Acta A* 129:256–267
- Arrizabalaga I, Gómez-Laserna O, Carrero JA, Bustamante J, Rodríguez A, Arana G, Madariaga JM (2015) Diffuse reflectance FTIR database for the interpretation of the spectra obtained with a handheld device on built heritage materials. *J Anal Methods* 7(3):1061–1070. <https://doi.org/10.1039/C4AY02189D>
- Auras M (2011) Leitfaden Naturstein-Monitoring. Nachkontrolle und Wartung als zukunftsweisende Erhaltungsstrategien. Fraunhofer-IRB-Verl, Stuttgart
- Bai Y, Thompson GE, Martinez-Ramirez S, Brüggerhoff S (2003) Mineralogical study of salt crusts formed on historical building stones. *Sci Total Environ* 302(1-3):247–251. [https://doi.org/10.1016/S0048-9697\(02\)00339-X](https://doi.org/10.1016/S0048-9697(02)00339-X)
- Barman I, Kong CR, Singh GP, Dasari RR (2011) Effect of photobleaching on calibration model development in biological Raman spectroscopy. *J Biomed Opt* 16(1):011004. <https://doi.org/10.1117/1.3520131>
- Basque Government, Department of Environment, Territorial Policy and Housing. www.ingurumena.ejgv.euskadi.eus
- Benavente D, Brimblecombe P, Grossi CM (2015) Thermodynamic calculations for the salt crystallization damage in porous built heritage using PHREEQC. *Environ Earth Sci* 74(3):2297–2313. <https://doi.org/10.1007/s12665-015-4221-1>
- Bicchieri M, Monti M, Piantanida G, Pinzari F, Sodo A (2011) Non-destructive spectroscopic investigation on historic Yemenite scriptorial fragments: evidence of different degradation and recipes for iron tannic inks. *Vib Spectrosc* 55(2):267–272. <https://doi.org/10.1016/j.vibspec.2010.12.006>
- Bionda D (2005) RUNSALT—a graphical user interface to the ECOS thermodynamic model for the prediction of the behavior of salt mixtures under changing climate conditions. <http://science.sdf.eu.org/runsalt/>
- BOPV, Boletín Oficial de País Vasco, No. 249, Decree 317 2002 of 30 December, art.13, sobre actuaciones protegidas de rehabilitación del patrimonio urbanizado y edificado, the Autonomous Community of the Basque Country
- Cardiano P, Sergi S, De Stefano C, Loppolo S, Piraino P (2008) Investigations on ancient mortars from the Basilian monastery of Fragalà. *J Therm Anal Calorim* 91(2):477–485. <https://doi.org/10.1007/s10973-006-8313-8>
- Castro K, Perez-Alonso M, Rodríguez-Laso MD, Fernández LA, Madariaga JM (2005) *Anal Bioanal Chem* 382(2):248–258. <https://doi.org/10.1007/s00216-005-3072-0>
- Chávez-Ulloa E, Camacho-Chab R, Sosa-Baz M, Castro-Borges P, Pérez-López T (2013) Corrosión process of reinforced concrete by carbonation in a natural environment and an accelerated test chamber. *Int J Electrochem Sci* 8:9015–9029
- City Council. Special protection plan of urban and built heritage: www.donostia.eus/
- C.N.R.-I.C.R (1980) *Materiali Lapidei: Campionamento*. Comas Grafica, Roma
- Colomban P (2011) The on-site/remote Raman analysis with mobile instruments: a review of drawbacks and success in cultural heritage studies and other associated fields. *J Raman Spectrosc* 43(11):1529–1535
- COM (2014) 477 final, towards an integrated approach to cultural heritage for Europe, Brussels
- Dariz P, Schmid T (2017) Ferruginous phases in 19th century lime and cement mortars: a Raman microspectroscopic study. *Mater Charact* 129:9–17. <https://doi.org/10.1016/j.matchar.2017.04.009>
- Doehne E, Price CA (2010) *Stone conservation: an overview of current research*. Getty Conservation Institute, Los Angeles
- Downs RT (2006) Program and abstracts of the 19th general meeting of the International Mineralogical Association in Kobe, Japan O03: 13
- Euskalmet. Basque Meteorological Agency, www.euskalmet.euskadi.net
- Flatt RJ, Caruso F, Aguilar Sanchez AM, Scherer GW (2014) Chemo-mechanics of salt damage in stone. *Nat Commun* 5(4823):4823. <https://doi.org/10.1038/ncomms5823>
- Fraquelo ML, Duran A, Herrera LK, Jimenez de Haro MC, Perez-Rodríguez JL (2009) Old and modern pigments identification from a 14th century sculpture by micro-Raman. *J Mol Struct* 924-926: 404–412
- Fregenal M, López Gómez J, Martín Chivelet J (2000) *Ciencias de la Tierra*. Diccionarios Oxford-Complutense, Madrid
- García-Garmilla, Rodríguez-Maribona I, Cano M, Zalbide M, Ibáñez-Gómez J A, Osa-Chans K, Garín S (2002). An analytical comparison of two commercial consolidating products applied to eocene sandstones from 16th and 19th century monuments in San Sebastián, northern Spain. *Mater Constr* 52: 5–12, 266, DOI: <https://doi.org/10.3989/mc.2002.v52.i266.331>
- Gázquez F, Rull F, Median J, Sanz C (2015) Linking groundwater pollution to the decay of 15th-century sculptures in Burgos Cathedral (northern Spain). *Environ Sci Pollut Res* 22(20):15677–15689. <https://doi.org/10.1007/s11356-015-4754-6>
- Gázquez F, Rull F, Sanz-Arraz A, Medina J, Calaforra JM, De las Heras C, Lasheras JA (2017) In situ Raman characterization of minerals and degradation processes in a variety of cultural and geological heritage sites. *Spectrochim Acta A* 172:48–57. <https://doi.org/10.1016/j.saa.2016.04.035>
- Giakoumaki A, Osticioli I, Angos D (2006) Spectroscopic analysis using a hybrid LIBS-Raman system. *Appl Phys A Mater* 83:537–541
- Gipuzkoa Provincial Council, Historical Artistic and Archaeological Heritage: gipuzkoakultura.net
- Gómez-Laserna O, Olazabal M, Morillas H, Prieto-Taboada N, Martínez-Arkarazo I, Arana G, Madariaga JM (2013) In-situ spectroscopic assessment of the conservation state of building materials from a

- palace house affected by infiltration water. *J Raman Spectrosc* 44(9): 1277–1284. <https://doi.org/10.1002/jrs.4359>
- Gómez-Laserna O, Prieto-Taboada N, Morillas H, Arrizabalaga I, Olazabal M, Arana G, Madariaga JM (2015) Analytical study to evaluate the origin and severity of damage caused by salt weathering in a historical palace house: the attack of infiltration water. *Anal Methods* 7(11):4608–4615. <https://doi.org/10.1039/C4AY02632B>
- Graue B, Siegesmund S, Oyhantcabal P, Naumann R, Licha T, Simon K (2013) The effect of air pollution on stone decay: the decay of the Drachenfels trachyte in industrial, urban and rural environments—a case study of the Cologne, Altenberg and Xanten cathedrals. *Environ Earth Sci* 69(4):1095–1224. <https://doi.org/10.1007/s12665-012-2161-6>
- Hopkinson L, Rutt K, Kristova P, Blows J, Firth C (2015) Sourcing limestone masonry for restoration of historic buildings, a spectroscopic pilot study. *J Cult Herit* 16(6):822–830. <https://doi.org/10.1016/j.culher.2015.03.007>
- Jiménez Roca E, Ruiz-Conde A, Sánchez-Soto PJ (2005) Preparation of stratigraphic sections (cross-sections): some practical aspects on the analysis of strates coming from Cultural Heritage materials (pigments and supports). *Bol Soc Esp Ceram* 44(6):382–278. <https://doi.org/10.3989/cyv.2005.v44.i6.333>
- Johansson LG, Linqvist O, Mangio RE (1988) Corrosion of calcareous stones in humid air containing SO₂ and NO₂. *Dur Build Mater* 5: 439–449
- Kortum G (1969) Reflection spectroscopy. Springer, Berlin. <https://doi.org/10.1007/978-3-642-88071-1>
- Kottek M, Grieser J, Beck C, Rudolf B, Rubel F (2006) World map of the Köppen–Geiger climate classification updated. *Meteorology* 15(3): 259–263. <https://doi.org/10.1127/0941-2948/2006/0130>
- Maguregui M, Prieto-Taboada N, Trebolazabala J, Goienaga N, Arrieta N, Aramendia J, Gomez-Nubla L, Sarmiento A, Olivares M, Carrero J A, Martinez-Arkarazo I, Castro K, Arana G, Olazabal M A, Fernandez L A, Madariaga J M (2010) Chemch first international congress chemistry for cultural heritage168
- Matović V, Erić S, Kremenović A, Colomban P, Serćković-Batočanin D, Matović N (2012) The origin of syngenite in black crusts on the limestone monument King's Gate (Belgrade Fortress, Serbia)—the role of agriculture fertiliser. *J Cult Herit* 13(2):175–186. <https://doi.org/10.1016/j.culher.2011.09.003>
- Medeghini L, Lottic PP, De Vito C, Mignardi S, Bersani D (2014) Micro-Raman spectroscopy and ancient ceramics: applications and problems. *J Raman Spectrosc* 45:1244–1250
- Miliani C, Rosi F, Daver I, Brunetti BG (2012) Reflection infrared spectroscopy for the non-invasive in situ study of artists' pigments. *Appl Phys A Mater Sci Process* 106(2):295–307. <https://doi.org/10.1007/s00339-011-6708-2>
- Nikolaus s A, Theoulakis P, Pitinis C (2009) Dry deposition effect of marine aerosol to the building stone of the medieval city of Rhodes, Greece. *Built Environ* 44(2):260–270. <https://doi.org/10.1016/j.builtenv.2008.03.001>
- Pérez-Alonso M, Castro K, Álvarez M, Madariaga JM (2004) Scientific analysis versus restorer's expertise for diagnosis prior to restoration process: the case of Santa Maria Church (Hermo, Asturias, North of Spain). *Anal Chim Acta* 524(1-2):379–389. <https://doi.org/10.1016/j.aca.2004.06.034>
- Pérez-Alonso M, Castro K, Madariaga JM (2006) Investigation of degradation mechanisms by portable Raman spectroscopy and thermodynamic speciation: the wall painting of Santa Maria de Lemoniz (Basque Country, North of Spain). *Anal Chim Acta* 571(1):121–128. <https://doi.org/10.1016/j.aca.2006.04.049>
- Price C A (2000) An expert chemical model for determining the environmental conditions needed to prevent salt damage in porous materials. European Commission Research Report No 11 (Protection and Conservation of European Cultural Heritage), Archetype Publications, London
- Prieto Taboada N, Gómez Laserna O, Martínez Arkarazo I, Olazabal MA, Madariaga JM (2012) Optimizations of two methods based on ultrasound energy as alternative to European standards from soluble salts extraction from building materials. *J Ultrasound Sonochem* 19(6):1260–1265. <https://doi.org/10.1016/j.ultsonch.2012.03.002>
- Prieto Taboada N, Gómez Laserna O, Martínez Arkarazo I, Olazabal M, Madariaga JM (2013) Relevance of cross-section analysis in correct diagnosis of the state of conservation of building materials as evidenced by spectroscopic imaging. *Anal Chem* 85(20):9501–9507. <https://doi.org/10.1021/ac4010315>
- Prieto-Taboada N, Ibarrondo I, Gomez-Laserna O, Martinez-Arkarazo I, Olazabal M A, Madariaga J M (2013) Buildings as repositories of hazardous pollutants of anthropogenic origin. *J Hazard Mater* 248–249: 451–460, 248-249, DOI: <https://doi.org/10.1016/j.jhazmat.2013.01.008>
- RILEM (1978), Crystallization test by total immersion (test V.1). Crystallization by partial immersion (test V.2). Proc Int Symp Deterioration and Conservation of Stone Monuments (UNESCO-RILEM), Paris
- Rodríguez-Maribona I, Zabalbide M, García Garmilla F, Ibáñez JA, Garín S (1999) Conservation study of the stone material used in the Culture House of Almirante Oquendo, in San Sebastian. *Mater Construcc* 49:19–30
- Rodríguez-Navarro C, Doehne E, Sebastian E (2000) How does sodium sulfate crystallize? Implications for the decay and testing of building materials. *Cem Concr Res* 30(10):1527–1534. [https://doi.org/10.1016/S0008-8846\(00\)00381-1](https://doi.org/10.1016/S0008-8846(00)00381-1)
- Saetta AV, Vitaliani RV (2004) Experimental investigation and numerical modeling of carbonation process in reinforced concrete structures: part I: theoretical formulation. *Cement Concrete Res* 34(4):571–579. <https://doi.org/10.1016/j.cemconres.2003.09.009>
- Sarmiento A, Perez-Alonso M, Olivares M, Castro K, Martinez-Arkarazo I, Fernandez LA, Madariaga JM (2011) Classification and identification of organic binding media in artworks by means of Fourier transform infrared spectroscopy and principal component analysis. *Anal Bioanal Chem* 399(10):3601–3611. <https://doi.org/10.1007/s00216-011-4677-0>
- Sawdy A, Price C (2004) Salt damage at Cleeve Abbey, England. Part I: a comparison of theoretical predictions and practical observations. *J Cult Herit* 6:125–135
- Sawdy A, Price C (2005) Salt damage at Cleeve Abbey, England. Part II: seasonal variability of salt distribution and implications for sampling strategies. *J Cult Herit* 6(4):361–367. <https://doi.org/10.1016/j.culher.2005.10.002>
- Schreiber M, Otto M, Fedotov PS, Wennrich R (2005) Dynamic studies on the mobility of trace elements in soil and sediment samples influenced by dumping of residues of the flood in the Mulde River region in 2002. *J Chemosphere* 61(1):107–115. <https://doi.org/10.1016/j.chemosphere.2005.02.096>
- Selwyn L (2004) Overview of archaeological iron: the corrosion problem, key factors affecting treatment, and gaps in current knowledge. Metal National Museum of Canberra, Australia
- Seo SS, Son SM, Lee CH, Bask K (2007) Compositional analysis of soluble salt in Bresle extraction from blocks in newbuilding ship-yards. ISST, Osaka
- Siegesmund S, Snethlage R (2011) Stone in architecture. Springer, Berlin. <https://doi.org/10.1007/978-3-642-14475-2>
- Steiger M, Asmussen S (2008) Crystallization of sodium sulfate phases in porous materials: the phase diagram Na₂SO₄-H₂O and the generation of stress. *Geochim Cosmochim Acta* 72(17):4291–4306. <https://doi.org/10.1016/j.gca.2008.05.053>
- Tournié A, Prinsloo LC, Paris C, Colomban P, Smith B (2011) The first in situ Raman spectroscopic study of San rock art in South Africa: procedures and preliminary results. *J Raman Spectrosc* 42(3):399–406. <https://doi.org/10.1002/jrs.2682>

- Tsui N, Flatt RJ, Scherer GW (2003) Crystallization damage by sodium sulfate. *J Cult Herit* 4(2):109–115. [https://doi.org/10.1016/S1296-2074\(03\)00022-0](https://doi.org/10.1016/S1296-2074(03)00022-0)
- Veneranda M, Aramendia J, Gómez-Laserna O, Fdez-Ortiz S, García-Camino L, Castro K, Azkarate A, Madariaga JM (2016) Characterization of archaeometallurgical artefacts by means of portable Raman systems: corrosion mechanisms influenced by marine aerosol. *J Raman Spectrosc* 48:258–266
- Vítek P, Jehlicka J, Howell GM, Edwards M (2013) Practical considerations for the field application of miniaturized portable Raman instrumentation for the identification of minerals. *Appl Spectrosc* 67(7):767–778. <https://doi.org/10.1366/12-06774>